Role of Porosity in Filtration: XIII. Behavior of Highly Compactible Cakes

Frank M. Tiller
Dept. of Chemical Engineering, University of Houston, Houston, TX 77204

Jae Hyun Kwon
Dept. of Environmental Science, Inje University, Kimhae 621-749, Korea

Compactibility of cakes and sediments is a key factor in the behavior of thickeners, filters, centrifuges and belt presses. Stress applied to cakes decreases porosity and increases resistance to flow. Empirical models presented here represent solidosity (volume fraction of solids) ϵ_s, specific resistance α and permeability K as functions of effective pressure p_s that are essential to developing mathematical models of thickening, filtration, and centrifugation. As suspensions are flocculated, the resulting aggregates become increasingly fragile and more compactible. Cake behavior undergoes substantial change, until it reaches a point at which increasing pressure unexpectedly no longer affects either % cake solids or filtrate volume vs. time. Traditional formulas for filtrate volume vs. time and average values of α, K, and ϵ_s were modified for highly compactible materials. The average value of α is proportional to the pressure drop across the cake and the average permeability is inversely proportional to Δp_c.

Introduction

Filtrate rate and liquid content of cakes are important factors in the design and operation of filters. A typical separation process begins with a treated suspension in which the particles occur as individual units or combined in an endless variety of flocs or aggregates. Interparticle forces ranging from electrostatic and van der Waals to strong ionic forces or simple geometric combinations of odd shapes lead to complex particulate structures that vary enormously in resistance to compressive forces. The relative effect of stress on increasing % solids and decreasing permeability is fundamental to prediction of the average % solids in cakes and the rate of production of solids and liquids.

The behavior of a cake depends on its initial structure laid down under a null stress and its subsequent response to pump pressure converted into frictional drag, surface forces developed by pistons or pressure-actuated impermeable diaphragms, and gravitational forces. A wide variation in behavior is found in cakes and sediments encountered in industrial and municipal solid/liquid separation operations. A highly aggregated structure is easily compacted. Stress applied to such cakes results in a decrease in porosity, an increase in resistance to flow, and a substantial decrease in permeability. The rate at which the permeability decreases with pressure has a profound effect on cake behavior. For highly compactible beds of fragile flocs or biosolids derived from municipal wastewater, pressures exceeding some low value (generally less than 1 atm) neither increase the filtrate flow rate nor decrease the average cake solidosity. It would appear that Darcy's law is violated in this instance. Filters are ineffective in reducing the liquid content of highly compactible flocs unless pressing techniques are employed after cake formation is completed.

Correspondence concerning this article should be addressed to F. M. Tiller.

Theory of Flow Through Compactible Beds

Basic elements for developing an approximate theory of flow through compactible, porous media in filters consist of Darcian-type equations that give the liquid flow rate as a function of the liquid pressure gradient and equations relating the cake structure to compressive loads due to frictional drag, gravitational and centrifugal body forces, and stresses produced by pistons and diaphragms used to squeeze cakes. For the simplest model in which it is assumed that the super-

ficial liquid flow rate q is constant throughout the cake at any instant, Darcy's formula takes the form

$$q = \frac{K}{\mu}\frac{dp_L}{dx} = \frac{1}{\mu\alpha}\frac{dp_L}{d\omega} \tag{1}$$

where p_L = liquid pressure, x = distance from the medium (Figure 1), ω = volume/unit area of solids in distance x, μ = viscosity, K (m^2) = permeability, and α (m^{-2}) = specific resistance. The differential volume of solids and the total volume of solids per unit area ω_c are given by

$$d\omega = \epsilon_s dx, \qquad \omega_c = \int_0^L \epsilon_s dx = \epsilon_{sav} L \tag{2}$$

where ϵ_s and ϵ_{sav} are respectively the local and average solidosities (volume fraction of solids). Replacing $d\omega$ in Eq. 1 by $\epsilon_s dx$ leads to the identity

$$\alpha K \epsilon_s = 1 \tag{3}$$

which shows that only two of these parameters are independent.

The structure of a cake as reflected by α, K, and ϵ_s is determined by the effective pressure p_s, which equals the total compressive load/unit area. In a typical pressure filtration in the absence of inertial and gravitational effects, p_s is determined by the accumulated frictional drag over the portion of the cake lying between x and L. For filters involving planar surfaces, the effective pressure p_s and the liquid pressure p_L are related by

$$p_L + p_s = p \qquad dp_s + dp_L = 0 \tag{4}$$

where p = applied pressure at cake surface (Figure 1) and it is assumed that point contact among particles exists and p_L is effective over the entire cross-sectional area.

As α, K, and ϵ_s are not functions of the liquid pressure, the differential dp_L that appears in the Darcy formulation must be replaced by $-dp_s$ in Eq. 1 to give

$$\frac{dv}{dt} = q = -\frac{K}{\mu}\frac{dp_s}{dx} = -\frac{1}{\mu\alpha}\frac{dp_s}{d\omega} \tag{5}$$

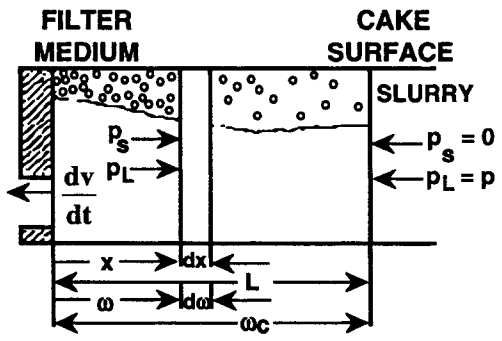

Figure 1. Cake with spatial (x) and material (ω) coordinates.

where v = filtrate volume/unit area and t = time. Because K and α are functions of p_s, the expressions in Eq. 5 can be integrated to yield q as a function of the pressure drop across the cake.

Empirical Constitutive Equations

The permeability K, specific resistance α, and solidosity (volume fraction of solids) ϵ_s can be related empirically to the effective or compressive pressure, p_s, by

$$(\epsilon_s/\epsilon_{so})^{1/\beta} = (\alpha/\alpha_o)^{1/n} = (K/K_o)^{-1/\delta} = 1 + p_s/p_a \tag{6}$$

where β, n, δ, and p_a are empirical parameters (compactibility coefficients) and ϵ_{so}, α_o, and K_o are values for an unstressed cake. The magnitudes of n and δ determine cake behavior under load. When both n and δ are greater than unity, a profound change in behavior takes place, and cake resistance R_c becomes proportional to the pressure drop Δp_c across the cake as the pressure increases. Doubling Δp_c ultimately leads to doubling of R_c with no change in the flow rate.

Constitutive relations similar to Eq. 6 represent the equilibrium relationships between the effective pressure and α, K, and ϵ_s. When there are large step changes in pressure, time is required for a porous cake to pass from one equilibrium state to another. Traditional filtration theory is based on the assumption that slowly changing conditions prevail in filtration operations. It then becomes possible to model a filtration as a series of steady states derived from ordinary differential equations and dependent on moving boundary conditions.

In expression of liquid from cakes through application of pressure by means of an impermeable membrane or piston (Svarovsky, 1990), however, the process is transient and requires the solution of nonlinear, partial differential equations (Tiller and Yeh, 1987). Shirato et al. (1970, 1986) developed a widely used method for correlating data obtained from expression experiments. Based on a combination of springs and a viscoelastic element, they obtained an analytical equation with parameters chosen to fit their experimental data. Kamst et al. (1998) developed equations for transient creep curves involving viscoelastic behavior of palm-oil filter cakes.

An important relation involving exponents in Eq. 6 can be obtained by forming the product $\alpha K \epsilon_s$ and substituting the result in Eq. 3 to yield

$$\alpha K \epsilon_s = \alpha_o K_o \epsilon_{so} (1 + p_s/p_a)^{\beta + n - \delta} = 1 \tag{7a}$$

As a consequence, the exponent must be zero and

$$\delta = n + \beta \tag{7b}$$

In line with all empirical expressions, the formulas in Eq. 6 should only be used in restricted pressure ranges. As cakes are compressed and ϵ_s increases, the structure becomes more rigid and values of β, n, and δ decrease. The shape and size of particles forming cakes with respect to elasticity, fragility, and degree of aggregation determine the response to stress. With unlimited increases in p_s in Eq. 6, calculated values of

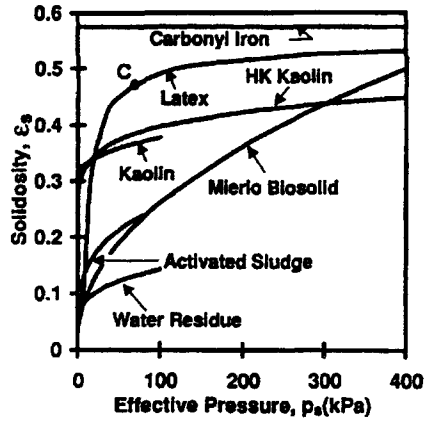

Figure 2. Effective pressure effect on local values of solidosity.

ϵ_s in excess of unity result. These values are clearly impossible but provide an extreme upper limit on pressures that could be used in the equations.

The behavior of materials with widely different properties is illustrated in Figures 2–4, where ϵ_s, α, and K are shown as functions of p_s. The materials can be classified into three categories as shown in Table 1.

Parameters for the materials illustrated in the figures are listed in Table 2 along with approximate ranges of effective pressure over which the values can be employed. With the exception of the polystyrene latex and carbonyl iron, the curves in Figures 2–4 have been derived from calculated values based on the empirical constitutive equations. The plots for the latex and carbonyl iron come directly from Grace's experimental data. Because of nonlinearity of the latex data, it is necessary to use different sets of parameters in different pressure intervals.

Plots of ϵ_s vs. p_s in Figure 2 provide a general view of the compactibility of various classes of materials. The solidosity of the iron carbonyl is essentially independent of applied stress and is classified as incompressible. Its behavior is typical of mixtures of dispersed spherical particles having a relatively modest range of sizes. The solidosity of dispersed or

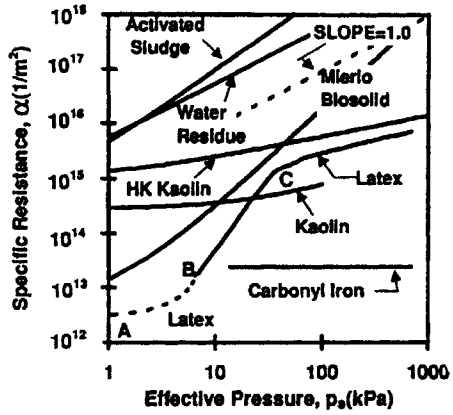

Figure 3. Effect of p_s on α.

Slopes of the logarithmic plots yield n, which is a measure of compactibility.

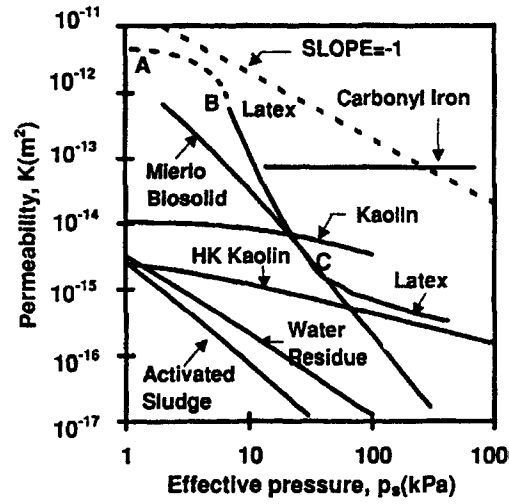

Figure 4. Effect of p_s on decreasing K.

Mierlo biosolids undergo a 10^5 change in local permeability over a 100-fold change in p_s.

relatively large particles depends principally on shape, with spherical types having an ϵ_s near 0.6.

The two kaolins exemplify moderately compressible materials. Whereas the null-stress solidosity ϵ_{so} of the iron carbonyl is close to 0.6, the corresponding values for the kaolins are near 0.3. At 100 kPa, ϵ_s of the Hong Kong pink kaolin increased to 0.39 in comparison to 0.37 for the second kaolin. A high degree of compactibility is demonstrated by the flocculated polystyrene latex, Mierlo biosolids (The Netherlands), activated sludge (Korea), and water residue (Korea).

In Figures 3 and 4, local values of specific resistance α and permeability K are shown as functions of p_s. Typical of incompressible cakes, both α and K for carbonyl iron are essentially independent of the effective stress. The two kaolins take an intermediate position with modest rates of change of α and K with p_s. When slopes of log α vs. log p_s exceed unity and slopes of log K vs. log p_s are less than negative unity, materials are classified as highly compactible. The activated sludge, water residue, Mierlo biosolids, and flocculated latex up to point C (Figures 2–4) fall into the highly compactible classification.

Table 1. Classification of Materials

Incompressible	
Carbonyl iron, grade E spheres in the 1.0–10 μm range with a surface average diameter = 5.7 μm	Grace (1953)
Moderately Compactible	
Hong Kong pink kaolin, 85% under 20 μm with 50% of the weight under 5–6 μm.	Shirato (1960)
Kaolin	Tiller and Horng (1983)
Highly Compactible	
Flocculated polystyrene latex. Nearly uniform 0.44 μm particles suspended in 0.01 molar $Al_2(SO_4)_3$	Grace (1953)
Mierlo biosolids. Biosolids flocculated with 1.5 wt. % on dry solid basis of Rohm KF975 polyelectrolyte	LaHeij (1994)
Activated sludge. Kimhae, Korea landfill leachate	Kwon (1995)
Water residue. Residue from clarifier used for potable water	Kwon (1995)

Table 2. Parameters for Constitutive Equations

Material	Hong Kong Kaolin*	Kaolin**	Mierlo Biosolid†	Activated Sludge‡	Water Treatment Residue‡	Carbonyl Iron Grade E††
ϵ_{so}	0.27	0.32	0.03	0.05	0.035	0.575
α_o, m^{-2}	1.15×10^{15}	2.88×10^{14}	4.02×10^{12}	3.62×10^{14}	7.93×10^{14}	2.34×10^{13}
K_o, m^2	3.22×10^{-15}	1.09×10^{-14}	8.30×10^{-12}	5.53×10^{-14}	3.60×10^{-14}	7.45×10^{-14}
β	0.09	0.09	0.47	0.26	0.22	0.001
n	0.375	0.55	1.83	1.40	1.03	0.005
δ	0.465	0.64	2.30	1.66	1.25	0.006
p_a, kPa	1.370	19.0	1.0	0.19	0.17	—
Range of p_s, kPa	1000	100	600	82	100	1000

*Shirato (1960). Data analysis of the Hong Kong Kaolin can be found in Tiller and Leu (1980).
**Tiller and Horng (1983).
†LaHeij (1994).
‡Kwon (1995).
††Grace (1953).

The latex illustrates the general behavior of a super-compactible material undergoing a wide range of compression. The solidosity ϵ_s of the fragile flocs (Figure 2) undergoes a rapid increase from 0.05 to about 0.47 (point C) in the pressure range of 50–70 kPa. At that point, the bed is approaching its maximum state of consolidation, and ϵ_s increases more slowly with p_s in the region beyond point C. This behavior is reflected in Figures 3 and 4 where there is a 100-fold increase in α and a corresponding decrease in K in the region BC. This region of supercompactibility is followed by a region in which the highly compressed aggregates mimic the behavior of the moderately compactible Hong Kong pink kaolin. The parameters n and δ reach values close to 2.7 and 4.0, respectively.

The Mierlo biosolids appear to have a more robust structure than the latex. In Figure 3, the curve for the specific resistance of latex lies below the curve for the Mierlo biosolids. The permeability of latex is greater than that of the Mierlo biosolids (Figure 4) except at point C, where the permeabilities of the two materials are almost equal.

Compactibility Parameters as Functions of ϵ_{so}

The variation of β, n, and δ with ϵ_{so} (Table 2) suggests the possibility of developing analytical equations incorporating the relationships. The degree of compressibility of a filter cake depends on how the null-stress structure (as defined by ϵ_{so}, K_o, and α_o) responds to added stress. Increasing load on a matrix of particles ultimately results in a state of consolidation such that additional stress has little effect on ϵ_s. Approximate differences of solidosity in the null-stress (ϵ_{so}) and consolidated (ϵ_{sc}) states and the ratio $\epsilon_{sc}/\epsilon_{so}$ for several materials appearing in Table 2 are shown in Table 3. The difference ($\epsilon_{sc}-\epsilon_{so}$) and the ratio ($\epsilon_{sc}/\epsilon_{so}$) are measures of the degree of compactibility.

Table 3. Consolidated and Null-Stress Solidosities

Material	ϵ_{so}	ϵ_{sc}	$\epsilon_{sc}-\epsilon_{so}$	$\epsilon_{sc}/\epsilon_{so}$
Carbonyl iron	0.575	0.58	0.005	1.01
Hong Kong Kaolin	0.27	0.45	0.18	1.67
Water residue	0.035	0.20	0.165	5.71
Activated sludge	0.05	0.37	0.32	7.40
Mierlo biosolids	0.03	0.50	0.47	16.67

Plots of β and δ as functions of ϵ_{so} are shown in Figures 5a and 5b. In addition to the materials (■) appearing in Table 2, data for additional materials have been added. Tsai (1986) obtained values of β and δ as functions of ϵ_{so} for kaolin Flat D (Δ), which was treated with flocculants and dispersants, leading to values of ϵ_{so} ranging from 0.05–0.35. Data

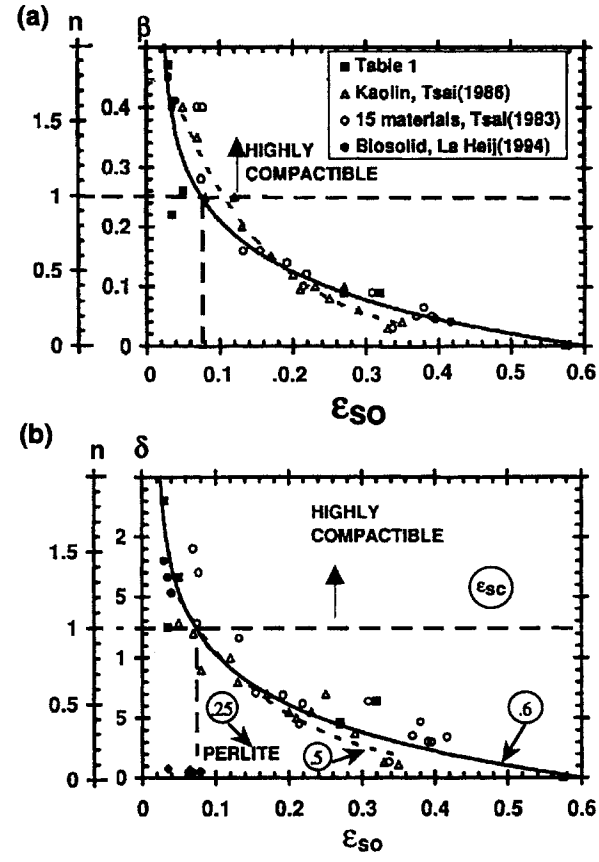

Figure 5. Compactibility parameters β, δ, and n as functions of the null stress, solidosity ϵ_{so}.

For materials having a consolidated solidosity ϵ_{sc} in the range of 0.5–0.6. Highly irregular perlite particles with ϵ_{sc} about 0.25 obeys a different relationship. The dotted lines in Figures 5a and 5b illustrate the behavior of flocculated and dispersed suspensions of commercial kaolin.

for 15 materials (○) appearing in the literature (Grace, 1953; Shirato et al., 1964; Tiller and Horng, 1983) were analyzed by Tsai (1983) and are shown in Figures 5a and 5b. An additional three points (●) reported by LaHeij (1994) are included in the graphs.

The shapes of both the β and δ vs. ϵ_{so} curves are similar and exhibit increasing values as ϵ_{so} decreases. Sharp increases in β and δ occur when $\epsilon_{so} < 0.1$. Equation 8 provides crude relationships among the parameters:

$$\ln\left[\frac{0.58}{\epsilon_{so}-0.02}\right] = 1.92\delta = 2.42n = 9.43\beta \tag{8}$$

For rule of thumb purposes, $\delta \approx 5\beta$ and $n \approx 4\beta$. The curves in Figure 5a and 5b have been constructed on the basis of the completely consolidated solidosity having a value of 0.6. The highly compactible region in which β and δ are rapidly increasing has been arbitrarily defined as lying in a range in which $\epsilon_{so} < 0.07$, $n > 1.0$, $\delta > 1.25$, and $\beta > 0.25$. The area above the dashed lines marks the region of high compressibility. Although Eq. 8 provides reasonable relationships over a wide range of ϵ_{so}, different materials will have different responses. It should only be used for rough estimates of materials having a consolidated solidosity, ϵ_{sc}, close to 0.5–0.6.

Particle shape has a significant effect upon ϵ_{sc}. Values of δ for an expanded perlite filter aid (Tsai, 1983) are shown in Figure 5b. Because of the highly irregular shapes of the particles, the value of ϵ_{sc} is low and in the neighborhood of 0.25. Consequently, the curve for perlite lies below the values predicted by Eq. 8. Every material would be expected to have a different relationship as illustrated by the dotted lines through the points corresponding to kaolin for which the value of ϵ_{sc} appears to lie in the range of 0.4–0.5.

Behavior of Highly Compactible Cakes

The effect of pressure on flow rate q and the average volume fraction of solids ϵ_{sav} of filter cakes is fundamental to operation and design. Integration of Eqs. 5 using the constitutive Eqs. 6 provides formulas relating q and ϵ_{sav} to the pressure drop across a cake, Δp_c. Variation of the liquid p_L and effective pressures p_s, is illustrated in Figure 6. The liquid enters the cake surface where $x = L$, $\omega = \omega_c$, $p_L = p$, and $p_s = 0$. The liquid pressure drops to p_1, which is required to overcome the resistance R_m of the supporting medium in accord with

$$p_1 = \mu q R_m \tag{9}$$

The effective pressure rises to $p - p_1 = \Delta p_c$ at $x = 0$ and $\omega = 0$. Combining the Darcy and constitutive equations and integrating across the cake yields

$$\mu q L = \int_o^{\Delta p_c} K dp_s = K_{av} \Delta p_c \tag{10}$$

$$\mu q L = \int_o^{\Delta p_c} K_o \left(1+\frac{p_s}{p_a}\right)^{-\delta} dp_s = \frac{K_o p_a}{1-\delta}\left[\left(1+\frac{\Delta p_c}{p_a}\right)^{1-\delta} - 1\right] \tag{11}$$

Repeating the integration with the material coordinate yields

$$\mu q \omega_c = \int_o^{\Delta p_c} \frac{dp_s}{\alpha} = \frac{\Delta p_c}{\alpha_{av}} \tag{12}$$

$$\mu q \omega_c = \int_o^{\Delta p_c} \frac{dp_s}{\alpha_o (1+p_s/p_a)^n} = \frac{p_a}{\alpha_o (1-n)}\left[\left(1+\frac{\Delta p_c}{p_a}\right)^{1-n} - 1\right] \tag{13}$$

These equations represent an instantaneous view of the cake and provide relationships among q, ω_c, L, and Δp_c. Dividing Eq. 13 by Eq. 11 leads to

$$\frac{\omega_c}{L} = \epsilon_{sav} = \epsilon_{so}\left(\frac{1-\delta}{1-n}\right)\frac{(1+p/p_a)^{1-n} - 1}{(1+p/p_a)^{1-\delta} - 1} \tag{14}$$

where $1/\alpha_o K_o$ has been replaced by ϵ_{so} in accord with Eq. 3; and it has been assumed that R_m and p_1 are small and $\Delta p_c \approx p$. It is clear from Eq. 14 that the average volume fraction of cake solids is heavily dependent both on the compactibility parameters and on the pressure.

For highly compactible materials with both $n > 1$ and $\delta > 1$, Eq. 14 can advantageously be placed in the form

$$\epsilon_{sav} = \epsilon_{so}\frac{\delta - 1}{n-1}\left[\frac{1 - 1/(1+p/p_a)^{n-1}}{1 - 1/(1+p/p_a)^{\delta-1}}\right] \tag{15}$$

As p increases, the last term in the denominator and numerator in the brackets becomes smaller and approaches zero, yielding

$$\epsilon_{sav} = \epsilon_{so}\frac{\delta - 1}{n-1} \tag{16}$$

The average solidosity of highly compactible cakes therefore approaches a constant value independent of pressure. This behavior is unexpected but is supported by experiment. Because of inherent problems of obtaining accurate values of ϵ_{so}, n, and δ, Eq. 16 does not yield highly accurate values,

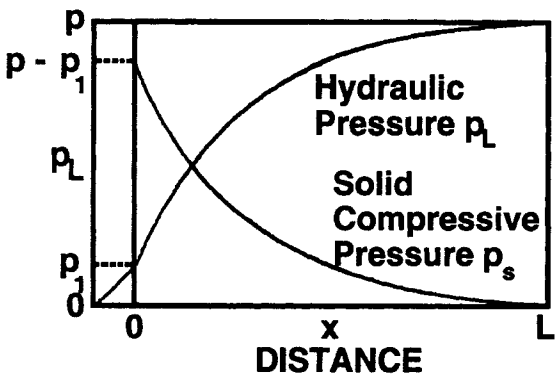

Figure 6. Variation of p_s and p_L within a filter cake.

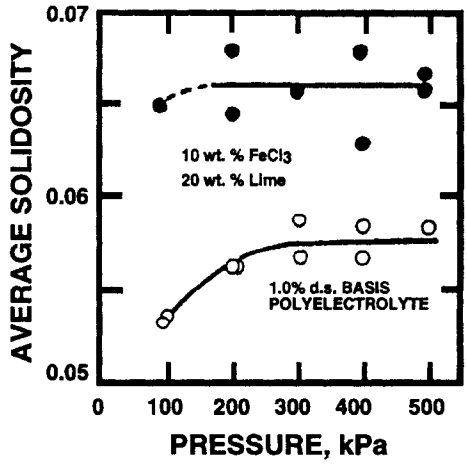

Figure 7a. Pressure effect in filtration of Eindhoven/ Mierlo sludge.

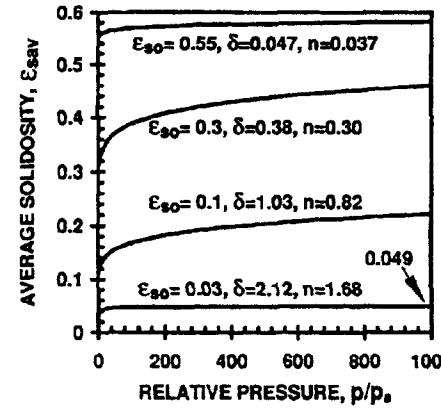

Figure 8a. Calculated effect of applied pressure on average solidosity of cakes.

With different degrees of compactibility as reflected by varying values of ϵ_{so}.

particularly when n is close to unity. In Figures 7a and 7b, ϵ_{sav} is plotted against the filtration pressure for Eindhoven/Mierlo biosolids (LaHeij, 1994) with two different flocculants and attapulgite clay. Although the scale in Figure 7a exaggerates the devivations in the experimental data, it is clear that the pressure had little effect when p exceeded approximately 100–200 kPa. Failure of high filtration pressure to increase the solid fraction of biosolids encountered in wastewater operations has led to the necessity of combining mechanical expression with filtration. Filter presses equipped with diaphragms for squeezing and belt presses are frequently used to express liquid from cakes of biosolids.

The results shown in Figure 7a relate to the formation of a highly compacted, resistant skin near the medium (Tiller and Yeh, 1987). LeHeij inserted probes into cakes and measured the hydraulic pressure at various depths. With the Eindhoven-Mierlo sludge, there was very little pressure lost over 90–95% of the cake, thus pointing to the existence of a skin. In highly compactible cakes, the resistant skin absorbs most of the pressure drop. The permeability of the resistant skin may be less than 1.0% of its value in the region in which there is little pressure loss. As little friction develops over a large fraction of the cake, there is virtually no compaction except in the skin. When the pressure drop is increased, most of the incremental pressure is absorbed in the resistant layer and ϵ_{sav} is not appreciably affected.

In Figure 7b, ϵ_{sav} and q are shown as a function of pressure for filtration of attapulgite (Tiller and Yeh, 1987). Beginning with the null solidosity approximately equal to 0.09, ϵ_{sav} increased to 0.2 and remained at that value up to the maximum pressure of 25,370 kPa (3,680 psi) in a severe test of the theory supporting Eq. 16. The rate was also unchanged by pressure.

Calculated values of ϵ_{sav} based on Eqs. 14 and 15 are provided in Figures 8a and 8b. The effect of filtration pressure (p/p_a) for systems of varying compactibility is illustrated in Figure 8a. For the highly compactible material ($\epsilon_{so} = 0.03$, $n = 1.68$, $\delta = 2.12$), the average solidosity rises rapidly to its limiting value (0.049) as predicted by Eq. 16. Even for the less compressible cakes with $\epsilon_{so} = 0.1$ and 0.3, the major increase in average solidosity occurs at relatively low pressures. High filtration pressures are not effective in increasing the % solids of highly compactible cakes. In order to increase the average solidosity, squeezing with fluid-activated diaphragms, pistons, rollers, or moving belts must be employed. When liq-

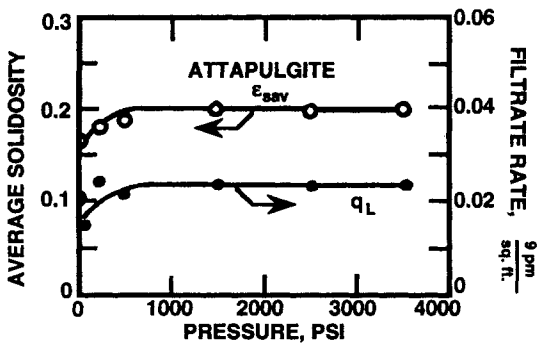

Figure 7b. Average solidosity and flow rate as a function of pressure drop during filtration.

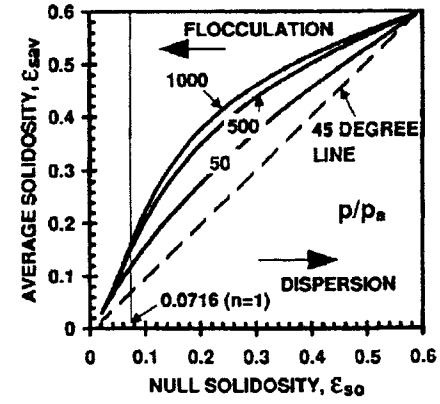

Figure 8b. Effect of flocculation and dispersion on ϵ_{sav} of a given system at different relative pressures.

As a system is flocculated, ϵ_{so} decreases.

Table 4. Comparing % Solids in Filtration and Expression at a Pressure of $p/p_a = 1{,}000$

ϵ_{so}	$\beta = \delta - n$	Average Solidosity		Fraction Removed
		Filtration	Expression	
0.03	0.44	0.049	0.63	0.92
0.10	0.21	0.22	0.43	0.63
0.30	0.08	0.46	0.52	0.21
0.55	0.01	0.58	0.59	0.04

uid is expressed from a cake by a fixed pressure applied to the cake surface, liquid flows out until the volume fraction of solids is uniform ($\epsilon_{sav} = \epsilon_s$) throughout the cake. At that point, the effective pressure is also uniform, and ϵ_s can be calculated using Eq. 6. As an example of the potential value of expression, Table 4 provides a comparison of solids in filtration and expression operations when $p/p_a = 1{,}000$. The last column represents the fraction of liquid in the filter cake which could be removed if an expression operation followed the filtration. With $\epsilon_{so} = 0.03$, expression could potentially remove 92% of the liquid left in the cake. As the compaction parameters β, n, and δ vary as the pressure increases, the values in Table 4 should be considered as providing estimates rather than precise values.

Whereas Figure 8a illustrates the effect of pressure on ϵ_{sav} of a given system, Figure 8b shows what would be expected as the system is flocculated or dispersed. Materials to the right with high values of ϵ_{so} represent dispersed systems while those with low values to the left correspond to flocculated systems. As dispersed systems are flocculated to increase the permeability, a simultaneous decrease occurs in the % of cake solids. Development of belt press filters in wastewater plants represents an empirical response to information available in Figure 8b. A high degree of flocculation results in a wet cake which requires an expression operation to increase the % solids. In the first stage of the belt press operation, filtration under gravity yields a relatively thin cake on one belt. The cake is then squeezed by a second belt as the two belts pass over a series of rollers.

Volume vs. Time for Highly Compactible Cakes

Conventional v vs. t equations must be modified for highly compactible materials. Equations 11 and 13 can be combined with an overall volume balance to produce an equation that can be integrated to give volume as a function of time. Volumetric balances over the slurry, cake, and filtrate are preferable to mass balances. However, with biosolids, where it is difficult to differentiate between combined and free water and true solids densities are not known, it is frequently necessary to employ mass balances. Beginning with a volumetric balance on a unit area basis

$$\text{slurry volume} = \text{cake volume} + \text{filtrate volume} \tag{17}$$

If the volume fraction of solids in the slurry is ϕ_s and the total volume of solids in the cake is ω_c, then

$$\frac{\omega_c}{\phi_s} = \frac{\omega_c}{\epsilon_{sav}} + v = L + v \tag{18}$$

Although ϵ_{sav} is assumed to be constant in conventional derivations, it varies when the pressure drop across the cake changes with time. Problems related to variable ϵ_{sav} can be avoided by elimination of L and ω_c. Solving for v in Eq. 18, multiplying by μq, and eliminating L and ω_c with Eqs. 10 and 12 leads to

$$\mu q v = \int_o^{\Delta p_c} \left(\frac{1}{\phi_s \alpha} - K \right) dp_s \tag{19}$$

Substituting for Δp_c and solving for v

$$v = \frac{1}{\mu q} \int_o^{p - \mu q R_m} \left(\frac{1}{\phi_s \alpha} - K \right) dp_s \tag{20}$$

This equation can be solved numerically to give v as a function of $q = dv/dt$. The time can then be obtained from the integral

$$t = \int_o^v dv/q \tag{21}$$

The area under a plot of $1/q$ vs. v yields the time. Substituting the integrated forms of Eqs. 11 and 13 into Eq. 20 produces

$$\frac{\mu q v}{p_a} = \frac{(1 + \Delta p_c/p_a)^{1-n} - 1}{\phi_s \alpha_o (1-n)} - K_o \frac{(1 + \Delta p_c/p_a)^{1-\delta} - 1}{1-\delta} \tag{22}$$

As long as $n < 1$ and $\delta < 1$, $(1-n)$ and $(1-\delta)$ are positive, and Eq. 22 can be used as is. However, when $n > 1$ and $\delta > 1$, both $(1-n)$ and $(1-\delta)$ are negative, and a profound change takes place in the nature of calculations based on Eq. 22. Rearranging Eq. 22 and substituting $K_o = 1/\alpha_o \epsilon_{so}$ leads to

$$\frac{\mu \alpha_o}{p_a} v \frac{dv}{dt} = \frac{1}{\phi_s (n-1)} \left[1 - \frac{1}{(1 + \Delta p_c/p_a)^{n-1}} \right] - \frac{1}{\epsilon_{so} (\delta - 1)} \left[1 - \frac{1}{(1 + \Delta p_c/p_a)^{\delta - 1}} \right] \tag{23}$$

As Δp_c increases, Eq. 23 approaches

$$\mu v \frac{dv}{dt} = \frac{p_a}{\phi_s (n-1) \alpha_o} - \frac{p_a K_o}{\delta - 1} \tag{24}$$

Using Eqs. 10 and 12 and assuming $n > 1$ and $\delta > 1$, it is possible to show that α_{av} and K_{av} approach the following forms as Δp_c increases.

$$\alpha_{av} = \alpha_o (n-1) \frac{\Delta p_c}{p_a} \tag{25}$$

$$K_{av} = K_o \frac{1}{\delta - 1} \frac{p_a}{\Delta p_c} \tag{26}$$

Thus the average specific resistance is proportional to the pressure drop and the average permeability is inversely proportional to the pressure drop for highly compactible cakes. Combining Eqs. 24–26 gives

$$\mu v \frac{dv}{dt} = \frac{\Delta p_c}{\phi_s \alpha_{av}} - K_{av} \Delta p_c \tag{27}$$

The terms $\Delta p_c/\alpha_{av}$ and $K_{av}\Delta p_c$ are both constant and independent of pressure. Integrating Eq. 24 yields

$$v^2 = \frac{2}{\mu}\left[\frac{p_a}{\phi_s(n-1)\alpha_o} - \frac{p_a K_o}{\delta - 1}\right] t = c_1 t \tag{28}$$

This v vs. t relationship is independent of applied pressure. For highly compactible cakes with sufficiently large values of n and δ, increasing pressure beyond some minimum value has little effect on v vs. t. In Figure 9, a theoretical plot of $1/q$ vs. v based on Eq. 23 is shown for Mierlo sludge using parameters obtained from Table 2 with $\phi_s = 0.015$, $\mu = 0.001$ Pa·s and $R_m = 5\times10^{10}$ (1/m). The curve rapidly approaches a straight line with an intercept close to zero (Tiller et al., 1980). The curvature prior to point A takes place in a period of about 10 s. Although it is possible to calculate theoretical values for the first few seconds, it would be impractical to obtain the corresponding experimental results.

In Figure 10, volume vs. time data are shown for a City of Houston waste-activated sludge. After mixing diluted polymer with the sludge containing 3.62% by weight of solids, the slurry was poured into a filter and pressure applied with compressed nitrogen. Starting with an initial pressure of 34.5 kPa (5 psi), the pressure was increased in increments of 34.5 kPa at intervals of 400 s. The final pressure of 207 kPa was reached in the period of 2,000–2,400 s. Each time the pressure was increased, a slight jump in the filtrate volume occurred. Determination of the valve of c_1 in Eq. 28 normally is obtained by plotting t/v vs. v. A particularly severe test involves calculating t/v^2 at one point and using the result to predict the entire v vs. t relationship. At $t = 2{,}200$ s, $v = 0.061$ m^3/m^2; and $t/v^2 = 5.91\times10^5$ s/m^2. The resulting relationship between v and t is

$$v^2 = 1.69\times10^{-6} t \tag{29}$$

The squares in Figure 10 represent values calculated on the basis of Eq. 29. Although the fit is excellent, it is essential to be conservative in interpreting parabolic fits. Over limited ranges, many functions can be approximated by second degree polynomials. Sorensen and Hansen (1993), Bruus (1992), LaHeij (1994), and Yeh (1985) have provided data that support Eq. 28.

It is interesting to note that theoretically both incompressible and highly compactible materials have the same parabolic relationship between volume and time.

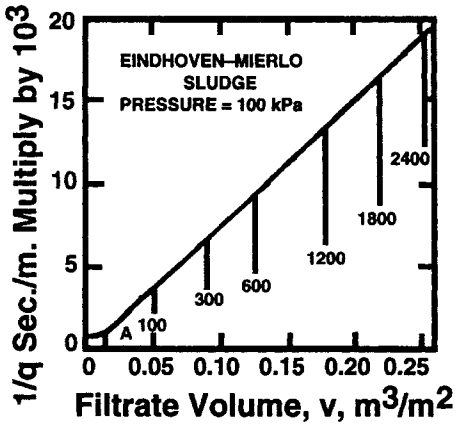

Figure 9. Calculated values for Eindhoven-Mierlo sludge with reciprocal rate $1/q$ as a function of filtrate volume.

The area under the curve yields the time of the filtration. Typical of highly compactible materials, the extrapolated straight line passes through the origin leading to a false R_m equal to 0.

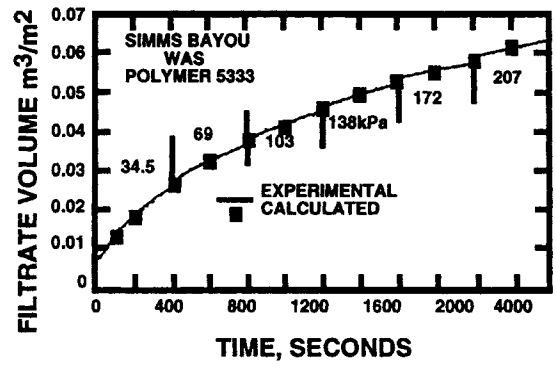

Figure 10. Experimental and calculated volume vs. time for stepped pressure filtration.

For Simms Bayou waste-activated sludge treated with polymer 5333.

Conclusions

High compactibility produces unexpected behavior in filter cakes that runs counter to normal engineering intuition. Failure to understand the phenomenon can lead to serious errors in designing new and operating existing equipment.

The presence of super-compactibility can be determined by either obtaining the null-stress solidosity ϵ_{so} or by using a stepped-pressure filtration experiment to ascertain the effect of pressure on filtrate volume vs. time. The null-stress solidosity is difficult to obtain experimentally because it is affected by many factors. It can be approximated by measuring the volume fraction (sediment volume) of a thin layer of sediment deposited from a suspension.

The compaction characteristics of cakes and sediments are at the heart of solid/liquid separation processes and merit increased research efforts. In the absence of a fundamental analysis of stress-strain characteristics of matrices of particles and aggregates improved empirical relationships represent a reasonable goal to pursue.

Acknowledgments

The authors wish to thank Ronald Clyburn of the City of Houston Wastewater Division for furnishing samples of waste activated sludge. Holly Chen of Espey and Associates and Ben Lopez, a student at the

University of Houston, performed the filtration experiments. Prof. dr. ing. P. J. A. M. Kerkhof kindly provided access to the extensive collection of data in Eindhoven Laboratories.

Notation

c_1 = constant, Eq. 28, m^2/s
K = permeability, m^2
K_{av} = average permeability, m^2
K_o = unstressed cake permeability, m^2
L = cake thickness, m
R_m = medium resistance, m^{-1}
x = distance from medium, m

Literature Cited

Bruus, J. H., "Filterability of Wastewater Sludge Flocs, Part III," PhD Diss., Aalborg Univ., Denmark (1992).
Grace, H. P., "The Resistance and Compressibility of Filter Cakes," *Chem. Eng. Prog.*, **49**, 303, 367 (1953).
Kamst, G. F., O. S. L. Bruinsma, and J. de Graauw, "Solid-Phase Creep During the Expression of Palm-Oil Filter Cakes," *AIChE J.*, **43**, 665 (1997).
Kamst, G. F., O. S. L. Bruinsma, and J. de Graauw, "Permeability of Filter Cakes of Palm Oil in Relation to Mechanical Expression," *AIChE J.*, **43**, 673 (1997).
Kwon, J. H., "Effects of Compressibility and Cake Clogging on Sludge Dewatering Characteristics," PhD Diss., Seoul National Univ., Korea (1995).
LaHeij, E. J., "An Analysis of Sludge Filtration and Expression," D. Eng. Diss., Technische Univ., Eindhoven, The Netherlands (1994).
Shirato, M., M. Sambuichi, and T. Murase, "Hydraulic Pressure Distribution in Filter Cakes under Constant Pressure Filtration," *Memoirs of the Faculty of Engineering*, Nagoya Univ., Japan, **16**(1/2), 68 (1964).
Shirato, M., "Filtration," D. Eng. Diss., Nagoya Univ., Japan (1960).
Shirato, M., T. Murase, T. Kato, and S. Fukaya, "Fundamental Analysis for Expression Under Constant Pressure," *Filt. & Sep.*, **7**, 277 (1970).
Shirato, M., T. Murase, M. Iwata, and S. Nakatsuka, "The Terzaghi-Voight Combined Model for Constant Pressure Consolidation of Filter Cakes and Homogeneous Semi-Solid Materials," *Chem. Eng. Sci.*, **41**, 3213 (1986).
Svarovsky, L., *Solid-Liquid Separation*, 3rd ed., Chap. 12, Butterworth (1990).
Sorensen, P. B., and J. A. Hansen, "Extreme Solid Compressibility in Biological Sludge Dewatering," *Wat. Sci. Tech.*, **28**, 133 (1993).
Tiller, F. M., J. R. Crump, and F. Ville, "A Revised Approach to the Theory of Cake Filtration," *Fine Particles Processing Proc.*, **2**, Amer. Inst. Min., Met. Pet. Engrs., New York (1980).
Tiller, F. M., and W. F. Leu, "Basic Data Fitting in Filtration," *J. Chinese Inst. Chem. Engrs.*, **11**, 61 (1980).
Tiller, F. M., and C. S. (S. H.) Yeh, "Role of Porosity in Filtration: XI. Filtration Followed by Expression," *AIChE J.*, **33**, 1241 (1987).
Tiller, F. M., and L. L. Horng, "Hydraulic Deliquoring of Filter Cakes, Reverse Flow in Filter Presses," *AIChE J.*, **29**, 297 (1983).
Tiller, F. M., N. B. Hsyung, and D. Z. Cong, "Role of Porosity in Filtration: XII. Filtration with Sedimentation," *AIChE J.*, **41**, 1153 (1995).
Tsai, C. D., "Theoretical and Experimental Studies in Filtration Mechanisms," MS Thesis, University of Houston, Texas (1983).
Tsai, C. D., "The Compressibility of Filter Cakes and Sediments," PhD Diss., University of Houston, TX (1986).
Yeh, S. H., "Cake Deliquoring and Radial Filtration," PhD Diss., Univ. of Houston, Texas (1985).

Manuscript received Dec. 16, 1997, and revision received July 29, 1998.